A comprehensive analysis of charge transfer effects on donor-pyrene (bridge)-acceptor systems using different substituents

Itamar Borges, Jr,[1,*] Roberta M. P. O. Guimarães,[1] Gabriel Monteiro-de-Castro,[1] Nathália M. P. Rosa,[1] Reed Niemann,[2] Hans Lischka,[2,*] Adelia J. A. Aquino[3,*]

[1] *Departamento de Química, Instituto Militar de Engenharia (IME), Rio de Janeiro, RJ 22290-270, Brazil*

[2] *Department of Chemistry and Biochemistry, Texas Tech University, Lubbock, TX 79409-1061, USA.*

[3] *Department of Mechanical Engineering, Texas Tech University, Lubbock, TX 79409-1021, USA.*

*Corresponding authors: itamar@ime.eb.br, adelia.aquino@ttu.edu, hans.lischka@univie.ac.at

Abstract

The alternant polycyclic aromatic hydrocarbon pyrene has photophysical properties that can be tuned with different donor and acceptor substituents. Recently, a D (donor) – Pyrene (bridge) – A (acceptor) system, DPA, with the electron donor N,N-dimethylaniline (DMA), and the electron acceptor trifluoromethylphenyl (TFM), was investigated by means of time-resolved spectroscopic measurements (J. Phys. Chem. Lett. 2021, 12, 2226−2231). DPA shows great promise for potential applications in organic electronic devices. In this work, we used the *ab initio* second-order algebraic diagrammatic construction method ADC(2) to investigate the excited-state properties of a series of analogous DPA systems, including the originally synthesized DPAs. The additionally investigated substituents were amino, fluorine, and methoxy as donors and nitrile and nitro groups as acceptors. The focus of this work was on characterizing the lowest excited singlet states regarding charge transfer (CT) and local excitation (LE) characters. For the DMA-pyrene-TFM system, the ADC(2) calculations show two initial electronic states relevant for interpreting the photodynamics. The bright S_1 state is locally excited within the pyrene moiety, and an S_2 state is localized ~0.5 eV above S_1 and characterized as a donor to pyrene charge transfer state. Density functional theory HOMO and LUMO energies were employed to assess the efficiency of the DPA compounds for organic photovoltaics. HOMO-LUMO and optical gaps were used to estimate power conversion and light-harvesting efficiencies for practical applications in organic solar cells. From the systems using smaller D/A substituents, compounds with the strong acceptor NO_2 substituent group show enhanced CT and promising properties for use in organic photovoltaics.

Keywords: Pyrene; D (donor)-Pyrene (bridge) – A (acceptor); Substituents; Charge transfer states; Organic electronics; Organic photovoltaics properties;

1 Introduction

Pyrene is an alternant polycyclic aromatic hydrocarbon (PAH) bearing four fused benzene rings which form an extended planar aromatic system. It shows high thermal stability, extensive electron delocalization, and behaves as an electron acceptor. It has a rich and unusual photophysical behavior showing anti-Kasha fluorescence from S_2 and even from higher excited states.[1-7] It is used in several important applications; for instance, as a dispersant to avoid the re-association of graphene sheets in the production of single (few) layer graphene sheets.[8] Pyrene and pyrenyl derivatives can behave as intramolecular charge transfer (ICT) molecules with applications in organic thin-films transistors and different types of organic electronic devices[9-14] due to the selective functionalization ability of the pyrene core.[1,15] Pyrene was first employed as a π −conjugated bridge in a donor (D)-pyrene (P (bridge))-acceptor (A) (DPA) organic dye for use as sensitizer in dye-sensitized solar cells, with diarylamine or indoline used as a donor, and cyanoacrylic acid as an electron acceptor[16] (Scheme 1). The syn- and anti-DPA systems can play the role of a donor in a dye-sensitized solar cell and adopt the same role in a bulk heterojunction (BHJ) of organic photovoltaic (OPV) systems.[17] In both cases, it transforms the incident solar radiation into excitons (bound electron-hole pairs), which are afterward separated by an interface involving an electron acceptor moiety (e.g., C_{60}) or TiO_2.

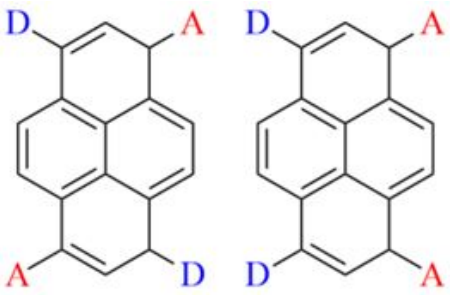

	DONOR	ACCEPTOR
DPA-1:	D = DMA	A = TFM
DPA-2:	D = NH_2	A = CN
DPA-3:	D = F	A = CN
DPA-4:	D = NH_2	A = NO_2
DPA-5:	D = OCH_3	A = NO_2

Scheme 1. The investigated anti- and syn-substituted pyrenes and the list of the investigated D/A substituent groups including N,N-dimethylaniline (DMA) and trifluoromethylphenyl (TFM).

ICT is a common and important photochemical process crucial in plant photosynthesis and the aforementioned applications. A molecule possessing an electron donor (D) and electron acceptor (A) connected by a single bond is the most straightforward ICT system.[18-20] Therefore, extending this idea by inserting donor (D) and acceptor (A) moieties into the pyrene core, the photophysical properties for a given application in optoelectronics can be tuned.[17]

The photophysical processes in photovoltaic cells can be characterized as follows. The excitons created by the absorbed light are converted into photogenerated charge transfer (CT) states (in most cases in an ICT process). Afterward, they are charge-separated at a donor-acceptor (D-A) junction from which the individual charge carriers may travel to the respective electrodes. In contrast with the scenario for traditional solar cell materials based on Si or Ge, the quantum efficiency for charge generation in pristine organic semiconductors can be quite low, about 1% in the first types developed before 2006. These quantum efficiencies have today increased to over 10%, but this value should increase even more for practical applications in organic electronics. For this reason, it is necessary to blend semiconductors with appropriate electron affinities and work functions to increase the quantum efficiency of the charge generation.[21] This is the donor-acceptor principle, which describes liquid-electrolyte and solid-state dye-sensitized solar cells, as well as polymer/fullerene (BHJs) solar cells.[22] Concerning DPA, as mentioned, the whole system can function as a sensitizer in a dye-solar cell, whose role is to absorb solar photons and inject the photoexcited electrons into the conduction band of an n-type semiconductor. DPA can also work as the donor part of a bulk heterojunction (BHJ) with an acceptor moiety like a C_{60} derivative or another molecule with a strong electron acceptor character.

In this work, we investigated theoretically DPA with trifluoromethylphenyl (TFM) as an electron acceptor group and N,N-dimethylaniline (DMA) as an electron donor, which was recently synthesized in two different arrangements (anti- and syn-DPA) and characterized using time-resolved fluorescence (TRF) spectroscopy by Park and coworkers.[17] Pyrene, in this case, plays the role of a bridge between the two types of substituents. It was found that CT processes occur in DPA because pyrene as a bridge mediates a strong electronic coupling between locally excited (LE) and CT states, with a solvent-independent enhanced and ultrafast CT within ~ 200 fs. The purpose of our work was to examine with state-of-the-art quantum chemical methods the electronic character of DPA systems because the interplay in donor-acceptor systems plays an important role in generating CT states. Other donor and acceptor groups, in addition to the original ones, were also studied in the present work. For the latter, we selected a set of small D/A groups because of the easier possibilities of their preparation; the investigated systems are depicted in Scheme 1. As additional donors, the amino, fluorine (donor owing to a conjugation effect, but it is usually an acceptor), and methoxy moieties were chosen. As acceptors, the nitrile and nitro groups were selected. A comparison of the effects of

these D/A combinations was made, especially regarding CT state generation in the experimentally investigated DMA/TFM pair of the original DPA. Since the creation and location of CT states play a crucial role, we used the *ab initio* second-order algebraic diagrammatic construction method (ADC(2)) for our calculations, thereby avoiding possible artifacts of overstabilization of CT states by the computationally more efficient time-dependent density functional theory (TD-DFT).[23,24] However, DFT HOMOs and LUMOs that include electronic correlation effects were used to estimate the characteristic parameters of an organic solar cell based on the different DPA compounds constructed from different donor and acceptor groups.

2 Methods

2.1 Properties

The π-conjugated material for OPV applications is characterized by some measurable properties that describe its usefulness and efficiency. The open circuit voltage V_{oc} is a critical parameter affecting the performance of organic solar cells, defined as the maximum current that can be extracted from an optical device. The open voltage delivered by a bulk heterojunction (BHJ) OPV under light illumination is limited by the low values of V_{oc}, which can be estimated by the empirical formula of Scharber:[22]

$$V_{oc} = \frac{1}{e}(|E^{Donor}HOMO| - |E^{PCBM}LUMO|) - 0.3\ eV \qquad (1)$$

where e is the elementary charge, and 0.3 is an empirical factor representing losses in the transport to the electrodes. The $E^{PCBM}LUMO$ (= – 3.7 eV) value refers to the standard acceptor in a BHJ, which can be changed to any other acceptor in an organic solar cell, including another type of OPV (e.g., dye-sensitized), thus being denoted now $E_{LUMO}^{acceptor}$. To produce a high value of V_{OC}, the HOMO level of the donor should have a lower energy (i.e., it has to be more stabilized), whereas the LUMO level of the acceptor should be higher in energy. It has been found that the Scharber formula does not reproduce the measured V_{oc} values very accurately,[25-27], but it is very useful to predict trends of V_{oc}.

In the Scharber model, the short circuit current density J_{sc} is related to the HOMO-LUMO gap (defined below as E_g), and the so-called fill factor FF which is set to 0.65 (65%). The latter is affected by several factors, being proportional to the realistic achieved performance (given by the product $V_{max}J_{max}$, the maximum values of V and J under a particular applied bias).[28] The power conversion efficiency (PCE) of solar cells is computed according to the equation:

$$PCE = \frac{V_{OC}J_{sc}FF}{P_{in}} \qquad (2)$$

where P_{in} is the incident power of the sun. The difference between the typical lower PCE of an OPV and a conventional semiconductor solar cell is attributed to the low values of FF. J_{sc}, the short circuit current, which has been improved in the novel low-bandgap materials.[28]

The light-harvesting efficiencies (LHE) of a π −conjugated polymer are given by:[29]

$$LHE = 1 - 10^{-f} \qquad (3)$$

where f is the optical oscillator strength of the first electronic transition ($S_0 \longrightarrow S_1$). To achieve high efficiency, the absorption spectrum of a donor polymer in an OPV material should match the solar radiation spectrum as much as possible.[30]

Quantum chemical methods can be employed to compute different types of band gaps,[31] which can be used to obtain different properties of π −conjugated systems for evaluating the material's potential for applications.

The band gap E_g is defined as

$$E_g = E_{LUMO} - E_{HOMO} \qquad (4)$$

which is a good approximation to the fundamental gap E_{fund} computed from the ionization potential and the electron affinity of the system. In extended systems, E_g corresponds to the difference between the valence and conduction bands. The smaller the E_g, the more significant

the chemical reactivity, the lower stability, and the easier the charge transfer (CT) process will be. In this case, the rate of CT increases, resulting in greater photon absorption hence increasing the PCE. Molecules bearing planar structure and push-pull arrangement (i.e., with an electron-withdrawing substituent on one side and an electron-donating substituent on the other) have a narrow band gap, high CT, and efficient absorption in the longer wavelength region.[32] Absorption maxima, similar to the band gap, are greatly influenced by extended conjugation and the electron-withdrawing effect of acceptor moieties.

The optical gap E_{opt} is the energy of the lowest electronic transition ($S_0 \rightarrow S_1$), usually the strongest in a π −conjugated material, accessible through the absorption of a single photon. E_{opt} is frequently lower than E_{fund} because in the excited state, in contrast to the ionized state, the electron and the hole remain electrostatically bound, thus forming an exciton.

DPA is a D-A polymer composed of donor and acceptor units. This kind of polymer has been largely used in organic solar cells and field effect transistors (OFETs) because they can be fine-tuned individually to improve performance. Generally, the internal dipole moment along the D-A copolymer chain is important for establishing charge transfer properties.[30] Furthermore, a weaker donor contributes to preserving a lower HOMO energy level. In contrast, a stronger acceptor can reduce the band gap by promoting intramolecular charge transfer (ICT) in a D-A copolymer.[33]

The dipole moment μ determines the morphology of the solar cell because it affects the polarity and the solubility of the molecule, thus, the FF; larger values of μ imply higher solubility in organic polar solvents.[33] The alignment of polar molecules is antiparallel because their opposite poles attract each other – this situation increases the self-assembly, hence decreases the molecular disorder. In this case, CT processes are improved, and charge recombination is reduced.

There is a phenomenological correlation between intramolecular dipole change and charge separation upon electronic excitation that can be used as a synthetic guideline for developing new materials.[34] The dipolar change (variation) between the ground and excited state is then given by

$$\Delta\mu_{ge} = \left[\left(\mu_{gx} - \mu_{ex}\right)^2 + \left(\mu_{gy} - \mu_{ey}\right)^2 + \left(\mu_{gz} - \mu_{ez}\right)^2\right]^{1/2} \quad (5)$$

in terms of Cartesian coordinates where the subscript g indicates the ground state electric dipole and e the same property for the excited state.

In the PTBn series of donor $\pi-$ conjugated polymers , Lu and coworkers showed that the total ground state dipole moment μ_g and the variation $\Delta\mu_{ge}$ correlate well with dynamic and solar cell data.[34,35] In particular, it is $\Delta\mu_{ge}$, and not μ_e, that correlates with PCE. Furthermore, the light-induced intensity of the ICT process is related to $\Delta\mu_{ge}$. In other words, the permanent dipole moment of a molecule with D/A moieties corresponds to a more favorable ICT effect.[30,35] Additionally, the dipole moment is essential in modulating the molecular energy level over the electronegativity, which is beneficial for charge separation in D-A blends.

2.2 Computational approach

The ground state (S_0) geometries were optimized by means of density functional theory (DFT) using the B3LYP functional[36] and the split-valence polarized SV(P) basis set.[37] The second-order algebraic diagrammatic construction (ADC(2)) *ab initio* method combined with the resolution of identity (RI) method[38,39] was employed for computing the electronic transition energies and oscillator strengths.[40-44] However, for calculating HOMO/LUMO energies, we have used DFT/B3LYP/SV(P) because it includes electron correlation in the molecular orbitals (MOs) in contrast to the Hartree-Fock method. The DFT MOs were employed for determining the relevant parameters of an OPV, as presented in Subsection 2.2. Solvent effects were included in the ADC(2) calculations using the continuum model COSMO[45,46] and a state-specific treatment of excited states.[47] The polar benzonitrile solvent ($\epsilon = 25.5$) was investigated. All calculations were performed using the program system Turbomole 7.5.[48]

Electron-hole maps for the transition from state n (usually the ground state $n = 0$) to state α in terms of fragments A and B were built from the omega matrices $\Omega_{AB}^{n,\alpha}$. They quantify the localization/delocalization degree, thus the amount of CT character.[49,50] These matrices are computed from the one-electron density transition matrices. The total amount of charge transfer q(CT) from fragment A to fragment B is determined as a sum over the matrix elements $\Omega_{AB}^{n,\alpha}$

for $A \neq B$; $\Omega_{AA}^{n,\alpha}$ gives the contribution from the excitation on the same fragment. When q(CT) $= 1$, there is a complete charge transfer of an electron, whereas for q(CT) $= 0$ the transition is a local excitation (Frenkel excitonic state) with the initial and final orbitals localized on the same fragm

Decomposition of the Ω matrix elements allows the determination of CT to and from pyrene and the substituents. For this analysis, several groups of electronic excitations were described: CT from substituents to pyrene (SPCT), CT from pyrene to the substituents (PSCT), CT between substituents (SSCT). Local excitation character is also described for pyrene (LEP) and the substituents (LES).

The natural transition orbitals (NTOs)[51] obtained from the one-electron transition density matrix provide a compact representation of the excited-state orbitals, thus of the electronic transitions, which removes the arbitrariness associated with a specific choice of molecular orbitals.[52] The Theodore program[53,54] was used for obtaining the NTOs and performing the CT analysis.

3 Results and discussion

3.1 Electronic spectra

The TRF experiments by Park and coworkers showed interesting results concerning the CT properties of the DPA-1 compounds. Given that these are fluorescence measurements, the results essentially refer to $S_1 - S_0$ transitions according to Kasha's rule[55,56] (fluorescence from higher states of pristine pyrene can only be achieved in gas phase collisionless regimes after transitions into higher excited states, as we have shown recently[7]). Their results for DPA-1 point to a strong polar electron distribution in the lowest excited singlet state of both anti and syn forms due to a pronounced CT character in contrast with the nonpolar nature of the ground state (the LE and CT states are supposed to be close in energy producing a strong electronic coupling between the two states). Therefore, the relaxation dynamics to the S_1 minimum should occur on one adiabatic energy surface in contrast with donor-pyrene-donor (DPD) systems[57] where a precursor-successor type CT has been found. To obtain an overview of the importance of CT character for the excited states of DPA compounds, we focus in this work on the analysis of vertical electronic excitations and the solvent effects on the extent of the CT. The use of the

ADC(2) method and solvation effects at the COSMO level should provide a balanced description of LE and CT states as has been shown in previous work.[58] This analysis should already give an interesting insight into the initial stages of the S_1 relaxation, and the electronic character of the lowest excited singlet states with an emphasis on the energetic ordering and coupling of the LE and CT states of DPA-1. The calculations on the smaller DPA compounds should provide insight into DPA compounds based on smaller acceptor and donor compounds and their interplay in CT phenomena without the possibility of larger charge delocalization.

Tables 1 and 2 display the computed ADC(2)/SV(P) vertical electronic spectra for the first five excited states of syn- and anti-DPA-1 (Scheme 1) for solvation by the polar solvent benzonitrile (BCN). Tables S1 and S2 of the Supporting Information (SI) collect the respective ADC(2)/SV(P) vertical gas phase electronic spectra. Tables S3 – S12 gather the same information for the small substituents. The five transitions of anti- and syn-DPA-1 have A' symmetry of the C_s point group and have π-π* character.

Table 1. Syn-DPA-1 (D – DMA, A – TFM, P – Pyrene) ADC(2)/SV(P) vertical absorption transitions in benzonitrile. Transition Energy (ΔE) in eV, oscillator strength (f), charge transfer number $q(CT)$ in e, assignment and contribution (in %) of the involved molecular orbitals, and character of CT. The q(CT) value is given for CT to pyrene (SPCT), and the total CT is in parentheses.

State	ΔE	f	q(SPCT)/q(CT)	Assignment[a]	Contribution (%)	Character[b,c]
S_1	2.549	1.421	0.360 / 0.629	H → L	93.6	LE(P)
S_2	3.014	0.594	0.564 / 0.760	H-1 → L	85.6	CT(D→P)
S_3	3.298	0.410	0.329 / 0.479	H → L+1	36.8	LE(P) CT(D→P)
				H → L+3	20.9	
				H-3 → L	19.5	
S_4	3.422	0.158	0.441 / 0.682	H-2 → L	85.6	CT(D→P)
S_5	3.878	0.841	0.268 / 0.578	H → L+4	46.7	CT(D→P) LE(P)
				H-3 → L	21.9	
				H → L+4	5.8	

[a] H – HOMO, L – LUMO.
[b] LE and CT mean, respectively, locally excited and charge transfer transitions.
[c] P, A, and D represent the pyrene core, acceptor, and donor moieties, respectively.

Table 2. Anti-DPA-1 (D – DMA, A – TFM) ADC(2)/SV(P) vertical absorption transitions in benzonitrile. Transition Energy (ΔE) in eV, oscillator strength (f), charge transfer number $q(CT)$ in e, assignment and contribution (in %) of the involved molecular orbitals, and character of CT. The q(CT) value is given for CT to pyrene (SPCT) and the total CT is in parentheses.

State	ΔE	f	q(SPCT)/q(CT)	Assignment[a]	Contribution (%)	Characterb[b,c]
S_1	2.538	0.418	0.359 / 0.620	H → L	93.4	LE(P)
S_2	3.044	0.171	0.607 / 0.822	H-1 → L	89.7	CT(D→P)
S_3	3.229	0.098	0.241 / 0.429	H-2 → L	35.8	LE(P)
				H → L+2	31.9	
				H-3 → L	14.6	
S_4	3.438	0.590	0.423 / 0.603	H-2 → L	51.0	LE(P)
				H → L+2	27.4	
S_5	3.839	0.006	0.228 / 0.680	H → L+1	69.1	LE(P)
				H-4 → L	9.2	

[a] H – HOMO, L – LUMO.
[b] LE and CT mean, respectively, locally excited and charge transfer transitions.
[c] P, A, and D represent the pyrene core, acceptor, and donor moieties, respectively.

All the computed transitions, both in the gas phase and solvated in benzonitrile (BCN), possess a nonnegligible CT character and a locally excited (LE) state character. In our analysis, we concentrate on the CT component donor substituent to pyrene (SPCT), which is expected to describe the character of the role of pyrene in the CT process best. For an analysis of the other CT contributions, refer to the following section. Our results confirm the experimental findings that anti- and syn-DPA-1 exhibit very similar CT processes (i.e., independent of the arrangement of the donor and acceptor moieties in the pyrene core). Upon solvation in polar benzonitrile (BCN), the character of the S_1 transition is preserved for both the syn- and anti-structures, but the charge transfer is slightly enhanced as indicated by the q(SPCT) values in Tables 1, 2, S1, and S2. As the discussion of omega matrices below shows, transition S_2 has its LE character mostly lost in solution, and the charge transfer magnitude q(SPCT) is preserved. For the transitions S_3 to S_5 in BCN, the anti-DPA-1 loses a bit in SPCT magnitude and character, whereas for syn-DPA-1 in BCN q(SPCT) increases (S_3 and S_5) or remains almost the same (S_4). The excitation energies of DPA-1 are red-shifted (i.e., decrease) upon solvation in BCN, excepting the S_5 state in syn-DPA-1 with a slight blue-shift (+0.02 eV). For both syn- and anti-DPA-1, the red-shift is about –0.1 eV, with two exceptions: syn-DPA-1 (S_3, –0.02 eV) and anti-DPA-1 (S_5, –0.05 eV). For the state of main interest (the bright S_1) in BCN, the optical oscillator strength remains the same for the syn conformation while decreasing for the anti by about 70%.

Park et al.[17] measured the UV absorption spectral peak in BCN at 2.42 eV (512 nm) for syn-DPA-1 and 2.40 eV (519 nm) for anti-DPA-1 (these experimental values were extracted from the absorption spectra in Figure S1 of their paper). Our computed vertical excitation energies of 2.538 eV (S_1) for syn-DPA-1 (Table 1) and 2.549 eV (S_1) for anti-DP-1 (Table 2) for BCN solvation are in good agreement with the experiment values. Both S_1 solvated states preserve the LE character at the pyrene core (Tables 1 and 2) found in the gas phase (Tables S1 and S2), as well as their CT character and the HOMO-LUMO assignment.

For the small substituents (Tables S3 – S12), five gas phase transitions ($S_1 - S_5$) were computed. We concentrate the discussion on the first transition (S_1) because this is the lowest bright state, except for syn-DPA-3 (D - F, A - CN), Table S6. For the small substituents, the anti- and syn-structures have similar oscillator strengths, except DPA-3 (D - F, A - CN), in which syn is dark and anti is bright. Thus, the conjugation properties of fluorine with the pyrene core are apparently much more favored in the anti-structure. Concerning the magnitude of charge transfer effects ($q(CT)$ values), DPA-2 (D – NH_2, A – CN) and DPA-3 have very small values ($\sim 0.1\ e$ and $\sim 0.2\ e$, respectively). This picture only changes when the strongly electron-withdrawing NO_2 group is used as an acceptor. In this case, DPA-4 (D – NH_2, A - NO_2) and DPA-5 (D – OCH_3, A - NO_2) have $q(CT)$ around $0.4\ e$. The strong acceptor NO_2 is synergetic for enhancing CT effects when bonded to a pyrene core, which could be explored in organic electronics.

3.2 Charge transfer analysis

A CT analysis based on plots of the Ω matrix according to the numbering of the five segments defined in Figure 1 for the original syn- and anti-DPA-1 systems was carried out. Figures 2 and 3 collect the most important NTOs for each electronic state of DPA-1 and the Ω matrix characterizing the excitonic and CT character of the excitation. For the other syn- and anti-DPA systems with smaller substituents, the same definition of the regions was used. The plots illustrate the probability of finding both an electron and a hole in a given segment of the molecule indicated by the location of the respective squares: excitons are related to the diagonal of the plots, whereas the CT character (or electron-hole separation) corresponds to the off-diagonal. The horizontal axis represents the hole position, and the vertical axis the electron.

The CT character $q(CT)$ of each transition is also collected in Tables 1 and 2, and for the small substituents, in Tables S3 – S10.

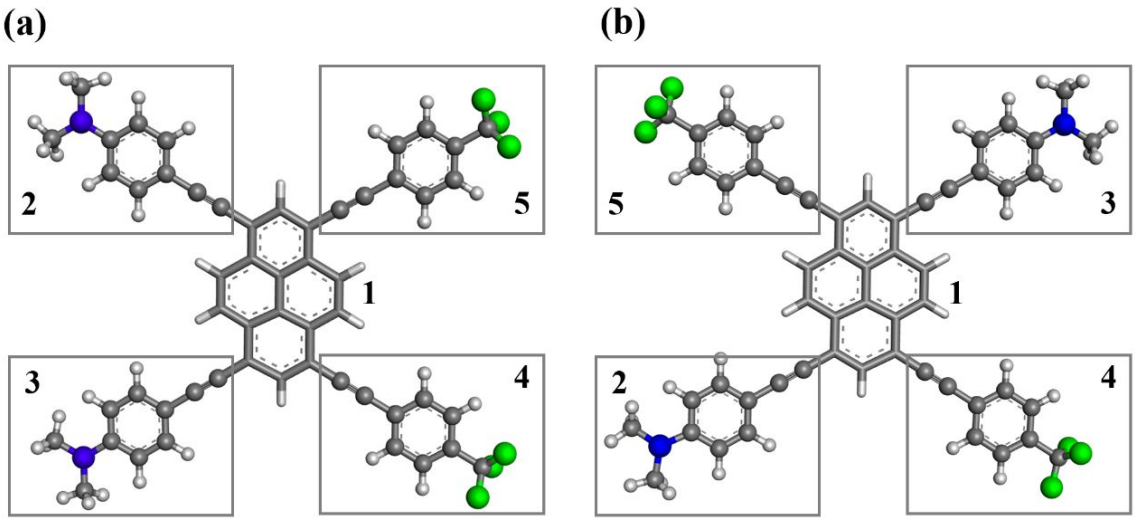

Figure 1. The fragments used for the syn and anti-DPA-1 molecules: (1) pyrene, (2) and (3) dimethylaniline (DMA) with the ethyne bridge, (4) and (5) trifluoromethylphenyl (TFM) with the ethyne bridge.

States	Occupied	Virtual	%	Ω Matrices
S_1	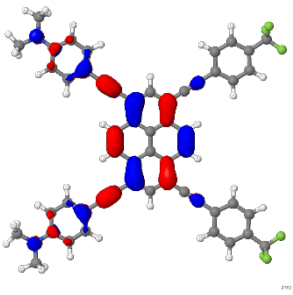	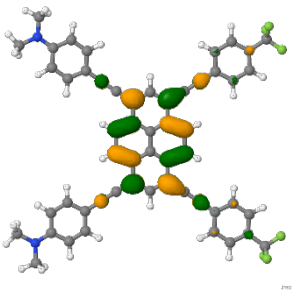	95	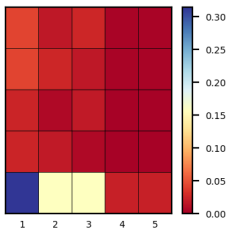 $q(CT) = 0.360\ (0.629)$
S_2	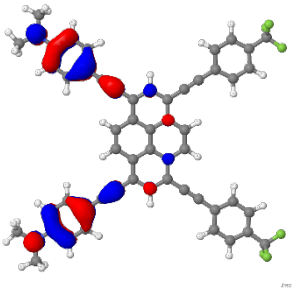	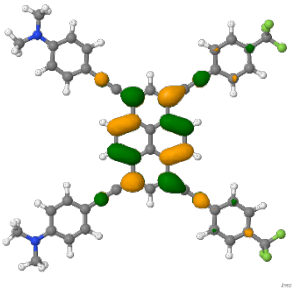	90	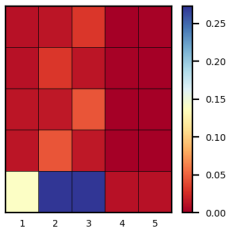 $q(CT) = 0.564\ (0.760)\ e$
S_3	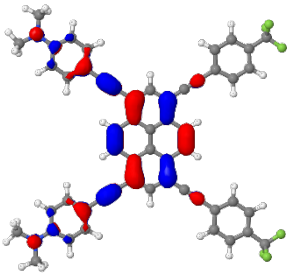	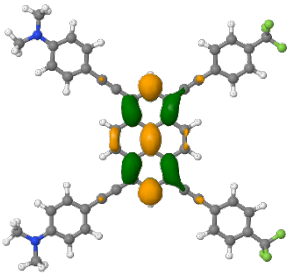	63	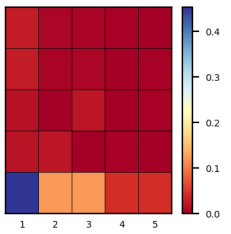 $q(CT) = 0.329\ (0.479)\ e$
	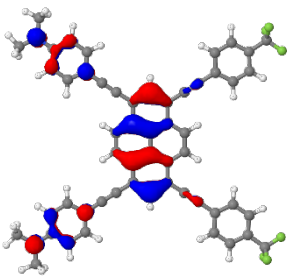	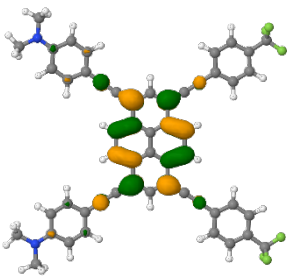	31	
S_4	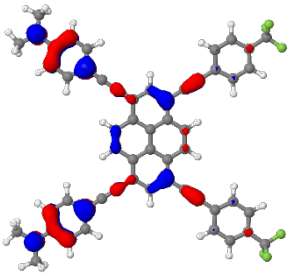	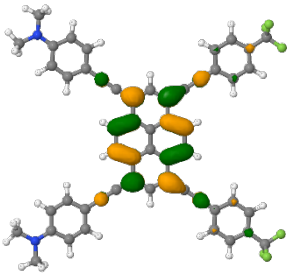	89	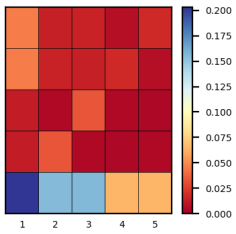 $q(CT) = 0.441\ (0.682)\ e$

S_5	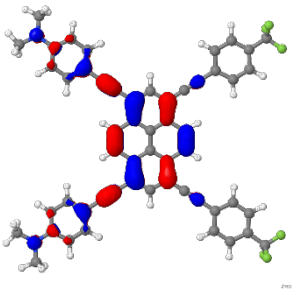	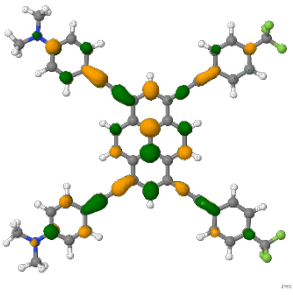	69	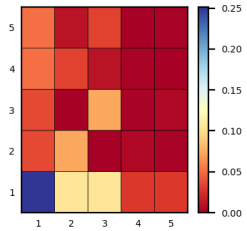 $q(CT)$ $= 0.268\ (0.578)\ e$

Figure 2. Syn-DPA-1 solvated in benzonitrile. ADC(2)/SV(P) natural transition orbitals (NTOs) of the singlet excitations and its Ω matrices. All transitions have A' symmetry of the C_s point group. The $q(CT)$ value is for the substituent to pyrene CT (SPCT); the total CT value is in parentheses.

States	Occupied	Virtual	%	Ω Matrices
S_1	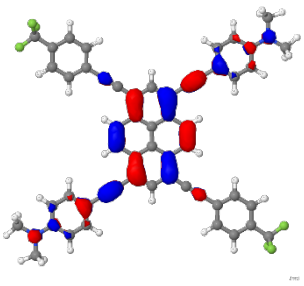	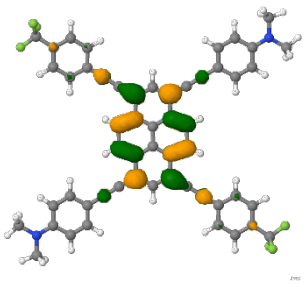	95	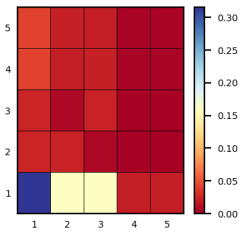 $q(CT)$ $= 0.359\ (0.620)\ e$
S_2	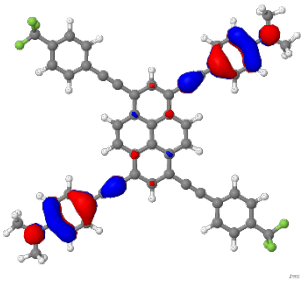	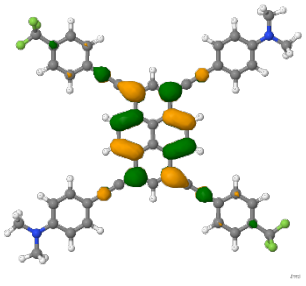	93	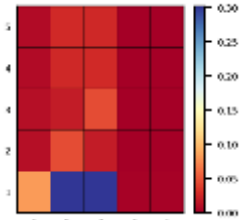 $q(CT)$ $= 0.607\ (0.822)\ e$
S_3	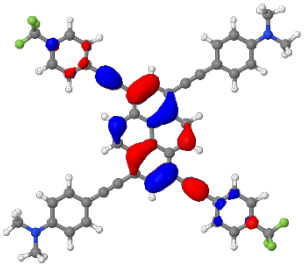	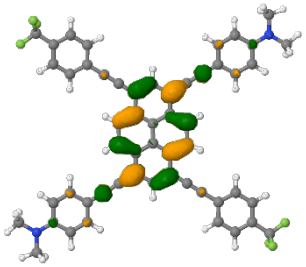	60	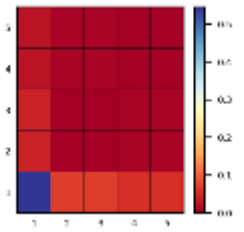

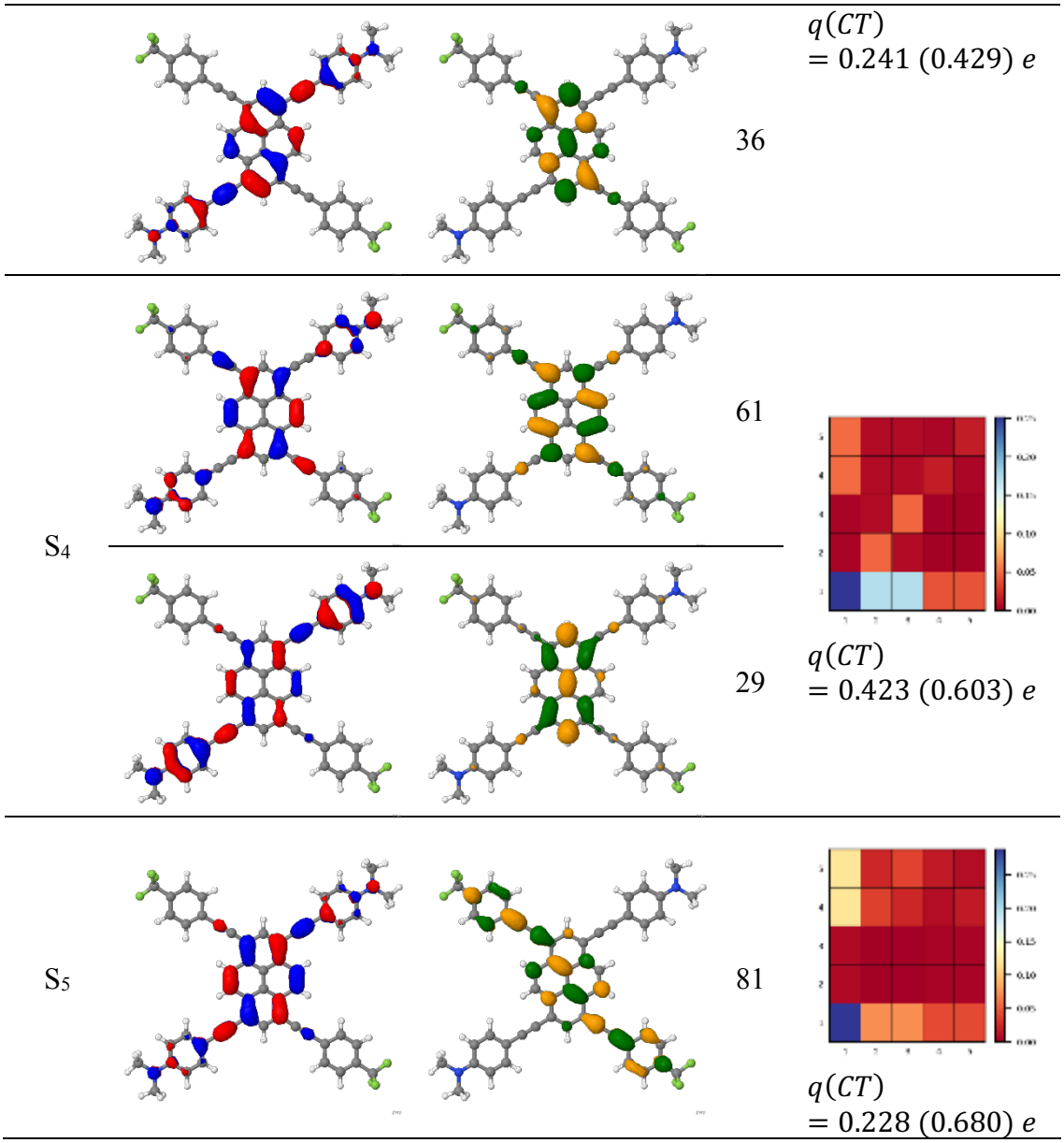

Figure 3. Anti-DPA-1 solvated in benzonitrile. ADC(2)/SV(P) natural transition orbitals (NTOs) of the singlet excitations and its Ω matrices. The $q(CT)$ value is for the substituent to pyrene CT (SPCT); the total CT value is in parentheses.

For both the syn- and anti-DPA-1 systems solvated in BCN (Tables 1 and 2 and Figures 2 and 3), the bright HOMO-LUMO S_1 state is of LE character located in the pyrene core, combined with a non-negligible SPCT character. The S_2 state possesses a dominant SPCT character involving the DMA donor and the pyrene core both for the syn- and anti-structures. The other excited states (S_3 – S_5) have a considerably smaller SPCT character than that of S_2.

Decomposition of the Ω matrix elements allows a more detailed fragment-driven CT description of DPA-1. For the S_1 state of syn-DPA-1 (Figure 4), for calculations with solvation effects, the two dominating processes are CT from the substituents to pyrene (SPCT, blue) and local excitation on the pyrene (LEP, orange). Excited state S_3 displays similar features. The largest SPCT is found in S_2 and S_4. CT between the substituents (SSCT, green) is a minor process and is found in approximately equal amounts for all states except S_3. For anti-DPA-1 (Figure 5), the same trends as with the syn conformer are also found, though, for all states except S_4, inter-substituent CT is a little larger. The gas phase CT decomposition for both conformers are shown in Figures S11 and S12. While some details are changed for the isolated systems, several overall trends, such as a large SPCT, are still present.

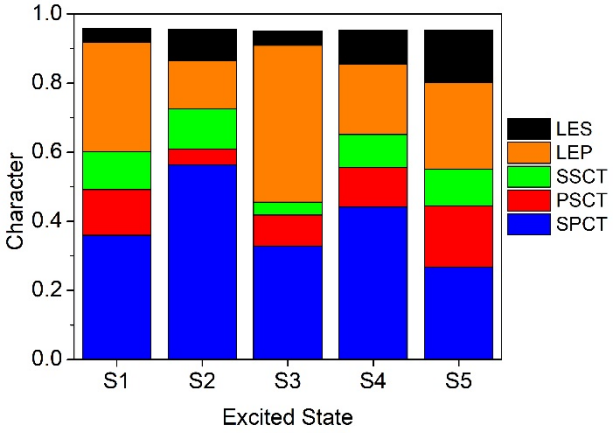

Figure 4. Syn-DPA-1 solvated in benzonitrile. ADC(2)/SV(P) excited state decomposition. SPCT – substituent-to-pyrene CT, PSCT – pyrene-to-substituent CT, SSCT – intersubstituent CT, LEP – local excitations on pyrene, LES – local excitations in the substituents.

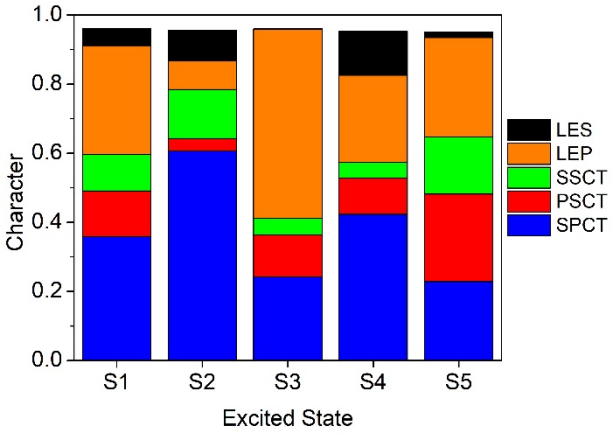

Figure 5. Anti-DPA-1 solvated in benzonitrile. ADC(2)/SV(P) excited state decomposition. SPCT – substituent-to-pyrene CT, PSCT – pyrene-to-substituent CT, SSCT – intersubstituent CT, LEP – local excitations on pyrene, LES – local excitations in the substituents.

For the smaller donor (NH_2, F, OCH_3) and acceptor (CN, NO_2) groups, due to their smaller sizes compared to the larger DMA and TFM groups in the DPA-1 systems, the CT character is, in most cases, considerably smaller (about one-third) compared with the original syn- and anti-DPA-1 systems (see Tables S3 – S10, Figures S3 – S10 and the discussion in the last paragraph of Section 3.1). Therefore, the smaller systems are not expected to have, in principle, the same photodynamical properties of DPA-1. The smaller size of the lateral groups results in the concentration of the occupied and virtual NTOs in the pyrene core. The exception to this behavior occurs for some transitions, in the sense of a more prominent CT character, when the strong electron acceptor NO_2 group is present. For DPA-5 (Figures S9 and S10), which has the donor moiety OCH_3 and the NO_2 acceptor, the S_3 and S_4 states interestingly have charge transfer involving the NO_2 moieties, whereas S_1 and S_2 have charge transfer from the pyrene core to the acceptor NO_2 groups.

3.3 Characteristic parameters of a solar cell

After discussing and characterizing the electronic structure and charge transfer effects of the first singlet transitions, we now analyze the syn- and anti-DPA systems (DPA-1 to DPA-5) for their relevant solar cell properties presented in the Methods section. For this purpose, we used the computed B3LYP/SV(P) HOMOs and LUMOs, whose energies are plotted in Figure 6.

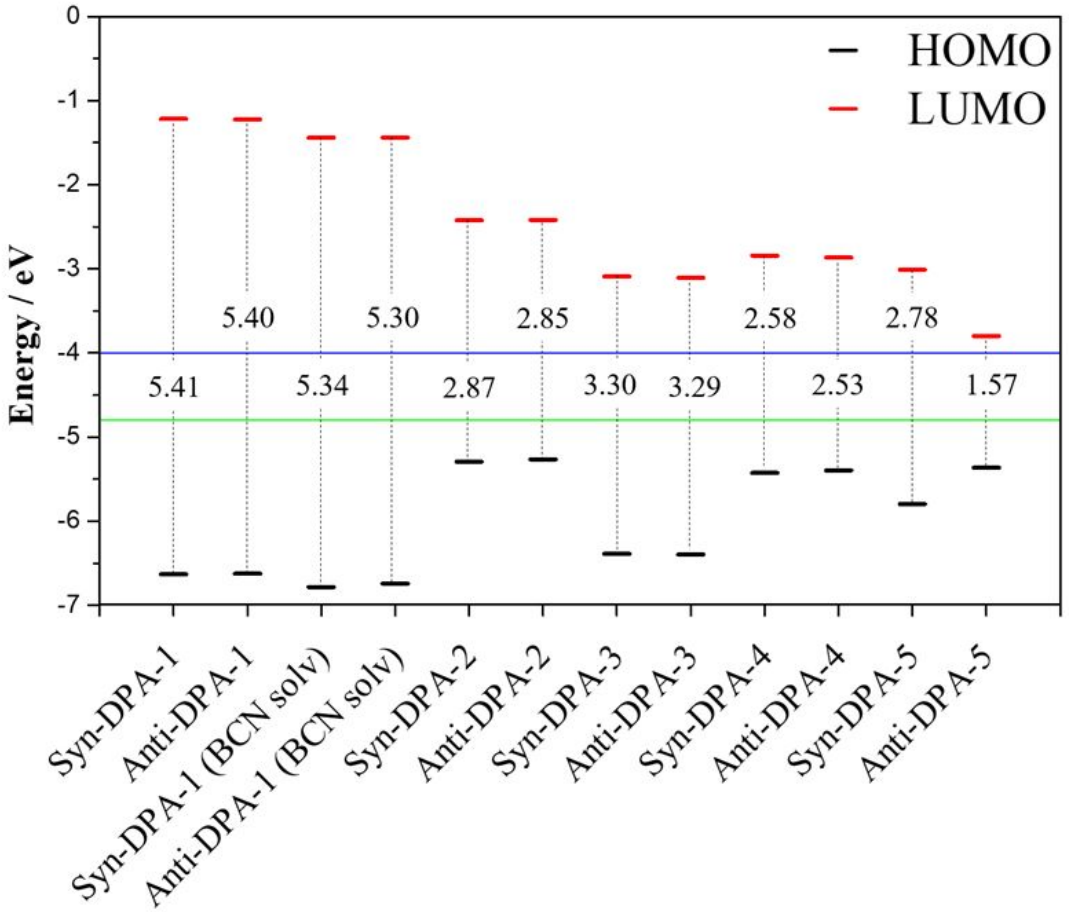

Figure 6. B3LYP/SV(P) HOMO and LUMO energies of the investigated systems. The blue line indicates the bottom of the conduction band of TiO_2 at 4.0 eV. The green line (4.8 eV) is the HOMO energy of the I^-/I_3^- electrolyte solution of a typical dye solar cell.

The largest band gaps E_g $(= E_{LUMO} - E_{HOMO})$ were found for the original DPA systems (syn and anti-DPA-1) with similar values (~5.4 eV). Values including BCN solvation are about 0.1 eV smaller. The gas phase band gaps for the other D-A substituted pyrene compounds (Scheme 1) are considerably smaller due to increasing HOMO and decreasing LUMO energies. Remarkably, the smallest band gap is obtained for anti-DPA-5, which combines the strong donor OCH_3 and the strong electron acceptor NO_2, and both have lone pairs. Interestingly, syn-DPA-5, which has the donor and the acceptor moieties on the same side of the pyrene core, has a band gap over 1 eV larger, a situation that concentrates electron density on this region. In contrast, for anti-DPA-5, the resonance effect of the NO_2 and OCH_3 substituents through the pyrene core is much more favored, thereby reducing E_g. A LUMO energy higher than the bottom of the TiO_2 conduction band is indispensable for allowing the removal of electrons from the dye and their injection into TiO_2. The HOMO energy should be lower than the I^-/I_3^- level to ensure that the electrolyte, thus the solar cell, functions in cycles

regenerating the oxidized dye molecules after injecting excited electrons into the TiO_2 electrode.

Table 3 collects the basic computed properties relevant to the efficiency considerations of OPV cells. The light-harvesting efficiencies (LHE) given by Eqn. (3) are substantially larger for the original syn-DPA-1 system in agreement with the experimental expectations.[17] However, anti-DPA-1 and several substituted systems with small groups also show substantial LHE values. In several cases, the syn arrangements favor a somewhat larger LHE. A unique situation occurs for syn-DPA-3 (F donor and CN acceptor), which has a much smaller LHE than anti-DPA-3 because the former has a much smaller optical oscillator strength f (0.012 compared to 0.31 of the latter). In some way, the highly electronegative F atom closer to the CN group without the pyrene core in between then promotes this large difference that favors the large LHE of anti-DPA-3 compared to syn-DPA-3.

Table 3. Selected properties for a donor of a solar cell for the investigated systems using the DFT/B3LYP method in the gas phase unless noted otherwise. See footnotes for the definitions of the properties of the table.

Systems	E_g / eV[a]	f_{osc}^{S1} [b]	E_{opt} / eV [c]	LHE [d]
Syn-DPA-1	5.41	1.4123	2.68	0.96
Anti-DPA-1	5.40	1.3875	2.66	0.96
Syn-DPA-1 (BCN solv)	5.34	0.4180	2.54	0.62
Anti-DPA-1 (BCN solv)	5.30	1.4214	2.55	0.96
Syn-DPA-2	2.87	0.5530	3.35	0.72
Anti-DPA-2	2.85	0.4530	3.23	0.65
Syn-DPA-3	3.30	0.0120	3.77	0.03
Anti-DPA-3	3.29	0.3080	3.64	0.51
Syn-DPA-4	2.58	0.5300	2.94	0.70
Anti-DPA-4	2.53	0.5060	2.84	0.69
Syn-DPA-5	2.78	0.6210	3.11	0.76
Anti-DPA-5	1.57	0.5380	3.00	0.71

[a] B3LYP/SV(P) band gap, E_g (Eqn. 4).
[b] ADC(2)/SV(P) optical oscillator strength of the first excited state S^1, $f_{osc}^{S_1}$.
[c] ADC(2)/SV(P) optical gap, E_{opt}.
[d] Light-harvesting efficiencies, LHE (Eqn. 3).

Figure 7 depicts the computed open circuit voltage V_{oc} values using Eqn. (1) and the LUMO values of the following acceptors (LUMO values in eV in parentheses): TiO_2 (–4.0

eV), $PC_{61}BM$ (–3.7) eV[32] and $PC_{71}BM$ (–3.9 eV).[59] A large V_{oc} value favors electron injection into the acceptors in an organic solar cell. The largest V_{oc} values were found for the original syn- and anti-DPA systems (syn-DPA-1 and anti-DPA-1), but DPA-3 (D - F, A – CN), and not far from it, DPA-5 (D – OCH_3, A – NO_2), have similar favorable values. The other systems have values about 1eV smaller and thus are less efficient for use in an organic solar cell. Given that the PCE is directly proportional to V_{oc}, the PCE values, thus the OPV efficiencies, have a similar behavior – see Table 4.

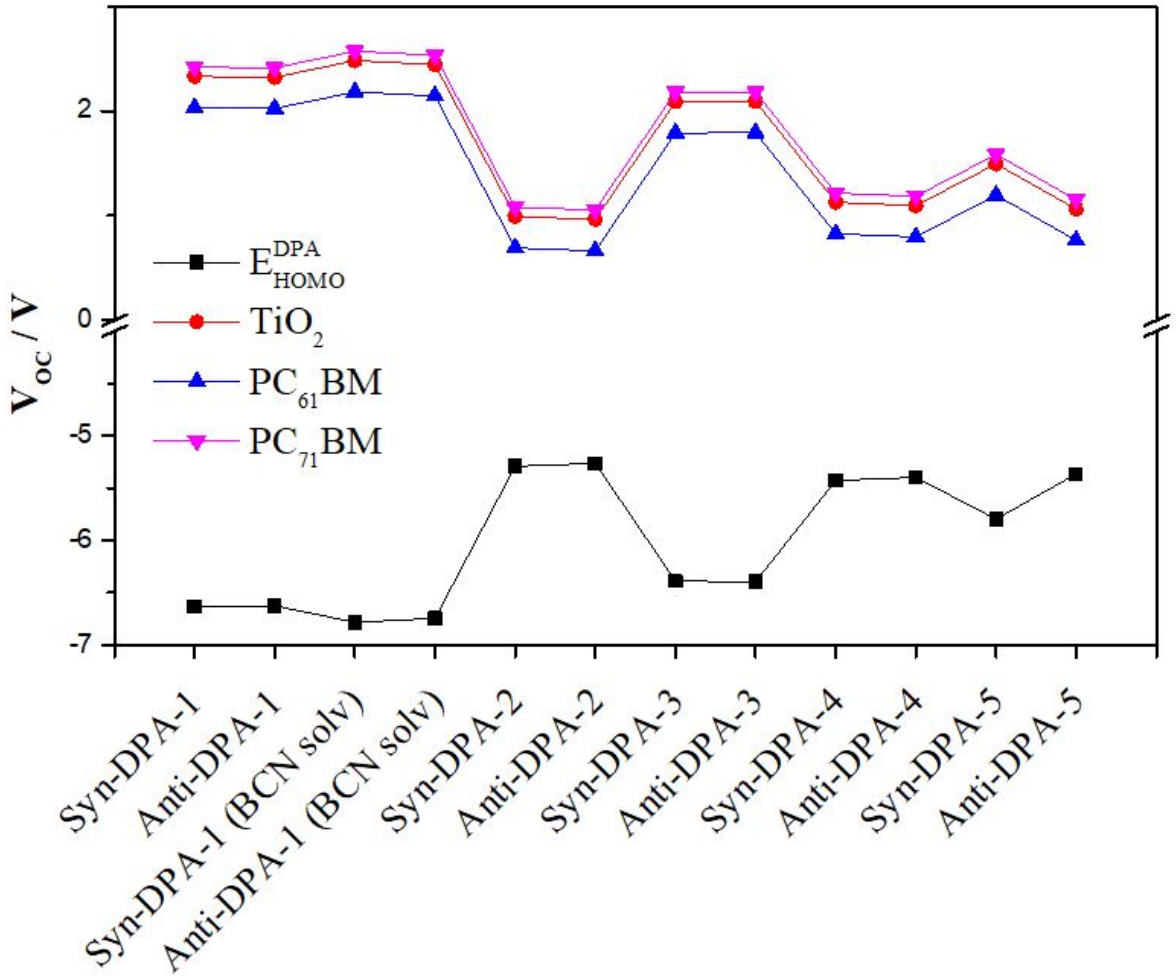

Figure 7. The computed open circuit voltage V_{oc} values using Eqn. (1). To compute V_{oc}, we used the LUMO values of typical electron-acceptors of an organic photovoltaic, namely, TiO_2 (–4.0 eV), $PC_{61}BM$ (–3.7) eV[32] and $PC_{71}BM$ (–3.9 eV).[59]

Table 4. Computed open circuit PCE values for TiO_2, $PC_{61}BM$, and $PC_{71}BM$ acceptors.

Systems	PCE (TiO_2)	PCE ($PC_{61}BM$)	PCE ($PC_{71}BM$)
Syn-DPA-1 (BCN solv)	0.01181	0.01038	0.01223
Anti-DPA-1 (BCN solv)	0.01162	0.01019	0.01205
Anti-DPA-2	0.00458	0.00316	0.00501
Syn-DPA-2	0.00471	0.00329	0.00514
Anti-DPA-3	0.00995	0.00853	0.01038
Syn-DPA-3	0.00994	0.00851	0.01037
Anti-DPA-4	0.00521	0.00379	0.00564
Syn-DPA-4	0.00536	0.00393	0.00578
Anti-DPA-5	0.00711	0.00568	0.00754
Syn-DPA-5	0.01099	0.00957	0.01142

The variation of the electric dipole moment between the ground and excited states, $\Delta\mu_{ge}$, Eqn. (6), correlates with the PCE, as well as with the light-induced intramolecular charge transfer (ICT) process.[34] Table 5 shows the computed $\Delta\mu_{ge}$ values for the syn-structures. The dipole moments for the anti-structures (not shown) are very small (less than 0.06 D) because of the quasi C_{2h} symmetry. Despite the quite low PCE values (around 1%), considering the potential for OPV applications of DPA-1, regarding this property, DPA-5 has a similar potential.

Table 5. Gas phase ADC(2) values of the dipole difference between the ground and excited states, $\Delta\mu_{ge}$, given by Eq. (5), in Debye, for the syn structures.

System	$\Delta\mu_{ge}$ [Debye]
Syn – DPA-1	9.440780
Syn – DPA-2	1.664489
Syn – DPA-3	0.394566
Syn – DPA-4	2.657030
Syn – DPA-5	2.979569

The $\Delta\mu_{ge}$ values confirm the original expectation that the synthesized syn - DPA-1 favors charge transfer, thus, a higher efficiency in an organic device. Syn-DPA-2 (D – NH_2, A – CN), and especially DPA-4 (D – NH_2, A – NO_2) and syn-DPA-5 (D – OCH_3, A - NO_2), though having $\Delta\mu_{ge}$ values about three times smaller than syn – DPA-1, have appreciable values. DPA-4 and DPA-5 have the strong electron-acceptor NO_2 moiety. To increase the

magnitude of $\Delta\mu_{ge}$, thus of charge transfer in a system bearing the pyrene core (and possibly any other π-conjugated core), one probably has to resort to larger donor and acceptor groups similar to the donor N,N-dimethylaniline (DMA) and the electron acceptor trifluoromethylphenyl (TFM) of the original DPA-1.

4 Conclusions

Using the *ab initio* ADC(2) method, we investigated the first five singlet electronic states of several DPA (donor–pyrene bridge–acceptor) systems in syn- and anti-structures with potential applications in organic electronics. The purpose was the elucidation and characterization of the relevant charge transfer states and the determination of organic photovoltaic (OPV) efficiency data for the compounds under investigation in this work. Incorporating different donor and acceptor groups into a pyrene core allows the fine-tuning of the photophysical properties of these systems.

In addition to the originally synthesized DPA with the electron donor N,N-dimethylaniline (DMA), and electron acceptor trifluoromethylphenyl (TFM), we studied the following smaller substituents, donors (amino, fluorine, and methoxy) and acceptors (nitrile and nitro). Good agreement with between calculated and experimental UV absorption energies was obtained for the original DPA-1 structures. Upon solvation by polar benzonitrile, charge transfer effects are somewhat enhanced. The first excited state (S_1) of DPA-1 is a locally excited (LE) state with a nonnegligible charge transfer (CT) character from the donor substituents to the pyrene core. The S_2 state of both syn- and anti-DPA-1 are of CT(D→Pyrene) type. Thus, our calculations present a slightly different picture in comparison to the original interpretation by Park et al..[17] The current calculations show the main part of the CT state in S_2 and the S_1 state as LE state (even though with significant CT character as well). Therefore, at least in the initial phase of the excited-state dynamics, the involvement of two electronic states (S_1(LE) and S_2(CT)) appear to occur, in contrast to the analysis of Park et al.[17] where a purely adiabatic picture of the CT dynamics is described. Excited-state dynamics in particular would be needed to resolve the question of the CT dynamics without this ambiguity.

For the small substituents in the gas phase, only the systems with the strong NO_2 electron acceptor have relevant charge transfer, The syn- and anti-structures have similar oscillator strengths, and the majority of the $S_0 \rightarrow S_1$ transitions are bright, with the exception

of DPA-3 (D – F, A – CN) in which syn is dark and anti is bright. A pictorial analysis of CT employing natural transition orbitals (NTOs) and omega plots identified the prominent role of the pyrene core bridge on the charge transfer processes.

The obtained properties of organic photovoltaics indicated that in addition to the original DPA-1, systems with the NO_2 acceptor substituent (DPA-4 and DPA-5, especially the latter) show promise for developing molecules with properties similar to the original DPAs for use in organic electronic devices. The present approach is general and available for investigating theoretically larger series of compounds for applications in organic electronics and computing relevant properties for photovoltaics.

Acknowledgments

I. B. thanks the Brazilian agencies CNPq (Grant numbers 304148/2018-0 and 409447/2018-8) and FAPERJ (Grant number E26/201.197/2021) for their support. We are grateful for the supply of computer time at the HPCC facilities of Texas Tech University.

Data Availability Statement

The data underlying this study are available in the published article and its supporting information.

Conflicts of Interest

There are no conflicts of interest to declare.

Supporting information

Gas ADC(2)/SV(P) tables of spectral data (transition energies, oscillator strengths, charge transfer values, and transition assignments), plots of NTOs, and omega matrices for all the DPA systems.

REFERENCES

[1] Figueira-Duarte, T. M.; Müllen, K. Chem Rev **2011**, 111, 7260.
[2] Itoh, T. Chem Rev **2012**, 112, 4541.
[3] Demchenko, A. P.; Tomin, V. I.; Chou, P.-T. Chem Rev **2017**, 117, 13353.
[4] del Valle, J. C.; Catalán, J. Phys Chem Chem Phys **2019**, 21, 10061.
[5] Malpicci, D.; Lucenti, E.; Giannini, C.; Forni, A.; Botta, C.; Cariati, E. Molecules **2021**, 26, 6999.
[6] Behera, S. K.; Park, S. Y.; Gierschner, J. Angewandte Chemie International Edition **2021**, 60, 22624.
[7] Braun, G.; Borges, I.; Aquino, A. J. A.; Lischka, H.; Plasser, F.; Monte, S. A. d.; Ventura, E.; Mukherjee, S.; Barbatti, M.; M., K. J Chem Phys **2022**, 157, 154305.
[8] Silva, N. J.; Borges, I.; Tone, P. A.; Green, M. J.; Lischka, H.; Aquino, A. J. A. Chem Phys **2019**, 527, 110468.
[9] Li, Y.; Liu, T.; Liu, H.; Tian, M.-Z.; Li, Y. Accounts Chem Res **2014**, 47, 1186.
[10] Neelambra, A. U.; Govind, C.; Devassia, T. T.; Somashekharappa, G. M.; Karunakaran, V. Phys Chem Chem Phys **2019**, 21, 11087.
[11] Scarongella, M.; Laktionov, A.; Rothlisberger, U.; Banerji, N. J Mater Chem C **2013**, 1, 2308.
[12] Bredas, J.-L.; Durrant, J. R. Accounts Chem Res **2009**, 42, 1689.
[13] Zhao, Y.; Liang, W. Chem Soc Rev **2012**, 41, 1075.
[14] Cole, J. M. J Chem Inf Model **2020**, 60, 6095.
[15] Yao, C.; Kraatz, H.-B.; Steer, R. P. Photochem Photobiol Sci **2005**, 4, 191.
[16] Yu, C.-C.; Jiang, K.-J.; Huang, J.-H.; Zhang, F.; Bao, X.; Wang, F.-W.; Yang, L.-M.; Song, Y. Org Electron **2013**, 14, 445.
[17] Park, J.; Sung, J.; Kim, D. J Phys Chem Lett **2021**, 12, 2226.
[18] Modesto-Costa, L.; Borges, I. Spectrochimica Acta Part A: Molecular and Biomolecular Spectroscopy **2018**, 201, 73.
[19] Yu, G.; Gao, J.; Hummelen, J. C.; Wudl, F.; Heeger, A. J. Science **1995**, 270, 1789.
[20] Yang, M.; Wei, W.; Zhou, X.; Wang, Z.; Duan, C. Energy Materials **2021**, 1, 100008.
[21] Bredas, J. L.; Beljonne, D.; Coropceanu, V.; Cornil, J. Chem Rev **2004**, 104, 4971.
[22] Scharber, M. C.; Mühlbacher, D.; Koppe, M.; Denk, P.; Waldauf, C.; Heeger, A. J.; Brabec, C. J. Adv Mater **2006**, 18, 789.
[23] Lischka, H.; Nachtigallova, D.; Aquino, A. J. A.; Szalay, P. G.; Plasser, F.; Machado, F. B. C.; Barbatti, M. Chem Rev **2018**, 118, 7293.
[24] Huix-Rotllant, M.; Ferré, N.; Barbatti, M. In Quantum Chemistry and Dynamics of Excited States; González, L.; Lindh, R., Eds.; Jonh Wiley & Sons Ltda.: Chichester, UK, **2020**, p 13.
[25] Lopez, S. A.; Sanchez-Lengeling, B.; de Goes Soares, J.; Aspuru-Guzik, A. Joule **2017**, 1, 857.
[26] Sahu, H.; Rao, W.; Troisi, A.; Ma, H. Adv Energy Mater **2018**, 8, 1801032.
[27] Sahu, H.; Yang, F.; Ye, X.; Ma, J.; Fang, W.; Ma, H. J Mater Chem A **2019**, 7, 17480.
[28] Jao, M.-H.; Liao, H.-C.; Su, W.-F. J Mater Chem A **2016**, 4, 5784.
[29] Sang-aroon, W.; Tontapha, S.; Amornkitbamrung, V. In Dye-Sensitized Solar Cells; Soroush, M.; Lau, K. K. S., Eds.; Academic Press, **2019**, p 203.
[30] Cui, Y.; Zhu, P.; Liao, X.; Chen, Y. J Mater Chem C **2020**, 8, 15920.
[31] Bredas, J.-L. Mater Horizons **2014**, 1, 17.
[32] Azeem, U.; Khera, R. A.; Naveed, A.; Imran, M.; Assiri, M. A.; Khalid, M.; Iqbal, J. ACS Omega **2021**, 6, 28923.

[33] Carsten, B.; Szarko, J. M.; Son, H. J.; Wang, W.; Lu, L.; He, F.; Rolczynski, B. S.; Lou, S. J.; Chen, L. X.; Yu, L. J Am Chem Soc **2011**, 133, 20468.
[34] Lu, L.; Yu, L. Adv Mater **2014**, 26, 4413.
[35] Modesto-Costa, L.; Borges, I.; Aquino, A. J. A.; Lischka, H. J Chem Phys **2018**, 149, 6.
[36] Becke, A. D. J Chem Phys **1993**, 98, 1372.
[37] Schafer, A.; Horn, H.; Ahlrichs, R. J Chem Phys **1992**, 97, 2571.
[38] Eichkorn, K.; Treutler, O.; Öhm, H.; Haser, M.; Ahlrichs, R. Chem Phys Lett **1995**, 240, 283.
[39] Sierka, M.; Hogekamp, A.; Ahlrichs, R. J Chem Phys **2003**, 118, 9136.
[40] Trofimov, A. B.; Schirmer, J. J Phys B-At Mol Opt Phys **1995**, 28, 2299.
[41] Hättig, C. In Advances in Quantum Chemistry; Jensen, H. J. Å., Ed.; Academic Press, **2005**, p 37.
[42] Dreuw, A.; Wormit, M. Wiley Interdiscip Rev-Comput Mol Sci **2015**, 5, 82.
[43] Tajti, A.; Tulipán, L.; Szalay, P. G. J Chem Theory Comput **2020**, 16, 468.
[44] Izsák, R. WIREs Computational Molecular Science **2020**, 10, e1445.
[45] Klamt, A.; Schuurmann, G. J Chem Soc-Perkin Trans 2 **1993**799.
[46] Klamt, A. Wiley Interdiscip Rev-Comput Mol Sci **2011**, 1, 699.
[47] Lunkenheimer, B.; Köhn, A. J Chem Theory Comput **2013**, 9, 977.
[48] Balasubramani, S. G.; Chen, G. P.; Coriani, S.; Diedenhofen, M.; Frank, M. S.; Franzke, Y. J.; Furche, F.; Grotjahn, R.; Harding, M. E.; Hättig, C.; Hellweg, A.; Helmich-Paris, B.; Holzer, C.; Huniar, U.; Kaupp, M.; Khah, A. M.; Khani, S. K.; Müller, T.; Mack, F.; Nguyen, B. D.; Parker, S. M.; Perlt, E.; Rappoport, D.; Reiter, K.; Roy, S.; Rückert, M.; Schmitz, G.; Sierka, M.; Tapavicza, E.; Tew, D. P.; Wüllen, C. v.; Voora, V. K.; Weigend, F.; Wodyński, A.; Yu, J. M.; Almlöf, J.; Faegri, F.; Korsell, K. J Chem Phys **2020**, 152, 184107.
[49] Plasser, F.; Lischka, H. J Chem Theory Comput **2012**, 8, 2777.
[50] Plasser, F.; Wormit, M.; Dreuw, A. J Chem Phys **2014**, 141.
[51] Martin, R. L. T. J Chem Phys **2003**, 118, 4775.
[52] Bäppler, S. A.; Plasser, F.; Wormit, M.; Dreuw, A. Phys Rev A **2014**, 90, 052521.
[53] Plasser, F. **2016**.TheoDORE 1.4: a package for theoretical density, orbital relaxation and exciton analysis. Available from http://theodore-qc.sourceforge.net/.
[54] Plasser, F. J Chem Phys **2020**, 152, 084108.
[55] Kasha, M. Discussions of the Faraday Society **1950**, 9, 14.
[56] B R Henry, a.; Kasha, M. Annu Rev Phys Chem **1968**, 19, 161.
[57] Sung, J.; Kim, P.; Lee, Y. O.; Kim, J. S.; Kim, D. T J Phys Chem Lett **2011**, 2, 818.
[58] Mattos, R. S.; Burghardt, I.; Aquino, A. J. A.; Cardozo, T. M.; Lischka, H. J Am Chem Soc **2022**, 144, 23492.
[59] Acquah, S. F. A.; Penkova, A. V.; Markelov, D. A.; Semisalova, A. S.; Leonhardt, B. E.; Magi, J. M. ECS Journal of Solid State Science and Technology **2017**, 6, M3155.